Dependence of interface states in the Si band gap on oxide atomic density and interfacial roughness

Yoshiyuki Yamashita
The Institute for Solid State Physics, The University of Tokyo, Roppongi, Minato-ku, Tokyo 106-8666, Japan

Akira Asano
The Institute of Scientific and Industrial Research, Osaka University, Mihogaoka, Ibaraki, Osaka 567-0047, Japan

Yasushiro Nishioka
Texas Instruments Tsukuba Research and Development Center Ltd., Miyukigaoka, Tsukuba, Ibaraki 305-0841, Japan

Hikaru Kobayashi
PRESTO, Japan Science and Technology Corporation, and the Institute of Scientific and Industrial Research, Osaka University, Mihogaoka, Ibaraki, Osaka 567-0047, Japan

(Received 13 July 1998; revised manuscript received 21 December 1998)

The energy distribution of interface states in the Si band gap present at ultrathin chemical oxide/Si(111) interfaces is obtained from measurements of x-ray photoelectron spectra under bias. The analysis of interface state spectra, together with the results obtained from measurements of Fourier-transform infrared attenuated total reflection spectra, atomic force micrographs, and synchrotron radiation ultraviolet photoelectron spectra, clarifies the relation of the interface states with the oxide atomic density and interfacial roughness. It is found that when the atomic density of the oxide layer is low (e.g., oxide formed in $HCl+H_2O_2$), an interface state peak appears near the midgap, which peak is attributable to isolated Si dangling bonds at the interface. For a high-atomic density oxide layer (e.g., oxide formed in HNO_3), interface state peaks are present above and below the midgap and are attributable to Si dangling bonds interacting weakly with a Si or oxygen atom in the oxide layer. The interface state density of an atomically smooth interface is much lower than that of an atomically rough interface. The interface is made smoother after oxidation with $HCl+H_2O_2$ than the initial surface, while it becomes rougher by oxidation with HNO_3 or $H_2SO_4+H_2O_2$. Consequently, the interface state density for the HCl oxide layer is lower than those for the HNO_3 and H_2SO_4 oxide layers.
[S0163-1829(99)00823-1]

I. INTRODUCTION

Studies of interface states present at Si/SiO_2 interfaces have been attracted much interest not only from an academic viewpoint but also concerning industrial application to metal-oxide-semiconductor (MOS) technology, because they seriously affect the electrical characteristics of MOS devices.[1] In spite of extensive studies, the origin of interface states has not been clarified on the atomic scale yet. One of the important reasons lies in the fact that interface states have been studied mainly using electrical technique, which gives little information on the atomic scale.

As the number of components per IC chip increases, gate oxide layers become thinner. The thickness of gate oxide layers will be reduced to 3 nm for 4-Gbit devices. For such ultrathin oxide layers, the interface properties (especially interface states) become more important than for thicker oxide layers. Therefore, the origin of interface states should be clarified on the atomic scale, which information is expected to be useful for the improvement of electrical characteristics of MOS devices. However, for MOS devices with an ultrathin oxide layer, the energy distribution of interface states cannot be obtained from electrical technique such as capacitance-voltage[2,3] (C-V) and conductance-voltage[4,5] (G-V) methods because a tunneling current flowing through the ultrathin oxide layer interrupts the electrical measurements.

We have recently developed a method for the observation of the energy distribution of interface states in the semiconductor band gap, on the basis of x-ray photoelectron spectroscopy (XPS) measurements under bias between the metal overlayer and the semiconductor substrate.[6–11] This method can be applied to MOS devices with an ultrathin oxide layer through which a high-density tunneling current flows. This spectroscopic method does not require assumptions such as an equivalent circuit, uniform distribution of dopant, etc., which are usually involved in the determination of the energy distribution of interface states using the electrical technique. Moreover, interface states in the whole band gap are observable as far as the interface Fermi level is shifted by a bias.

For a Si(111)-based MOS structure with a thick thermal oxide layer, interface state spectra with two peaks, one above and the other below the midgap, were observed.[12,13] On the other hand, only one peak was observed in the interface state spectra for a silicon oxide layer deposited on Si(111) by means of a remote plasma oxidation method.[14,15] These results indicate that the energy distribution of interface states depend on the oxide formation methods

It is reported that the microroughness at Si/oxide inter-

faces affects the interface state density.[16,17] The density of interface states for silicon oxide layers deposited on atomically flat Si(111) surfaces is as low as that for Si(100)/thermal oxide interfaces,[15] although the interface state density for Si(111)/thick oxide interfaces is usually higher than that for Si(100)/thick oxide interfaces.

In the present study, the energy distribution of interface states for Si(111)-based MOS devices with an ultrathin oxide layer formed in chemical solutions (chemical oxide) was obtained from XPS measurements under bias. Information on the structure of the chemical oxide layers was obtained from Fourier-transformed infrared attenuated total reflection (FT-IR-ATR) spectroscopy measurements, and that on the chemical bonding states near the Si/oxide interfaces from synchrotron radiation ultraviolet photoelectron spectroscopy (UPS) measurements. The surface morphologies before and after oxidation were observed by means of atomic force microscopy (AFM). On the basis of the comparison of the interface state spectra with these results, the origin of the interface states is discussed on the atomic scale.

II. EXPERIMENTS

MOS structure was fabricated from phosphorus-doped *n*-type floating zone Si(111) wafers with a resistivity of $\sim 10\ \Omega$ cm. The wafers were cut into 5×5-mm^2 pieces except for FT-IR-ATR measurements in which 20×50-mm^2 pieces were employed. After cleaning the wafers with an RCA method, atomically rough and smooth Si surfaces were prepared by following methods: For the production of atomically rough surfaces, the wafers were simply immersed in a 1% hydrofluoric acid (HF) solution for 30 s. For the preparation of atomically smooth surfaces, on the other hand, ~ 100 nm-thick silicon oxide layers were formed by heating the wafers at 1100 °C in a dry O_2 atmosphere for 1 h, followed by heat treatment in N_2 at 1100 °C for 20 min. The oxide layers thus formed were etched away by a 5% HF solution, and then the wafers were immersed in a 40% NH_4F solution for 15 min. It was reported[18] that the treatment with 40% NH_4F resulted in atomically smooth silicon surfaces covered fully with monohidride.

Silicon oxide layers were formed by the immersion of the Si wafers thus treated in following solutions:
(1) H_2SO_4:H_2O_2=2:1 at 110 °C for 10 min;
(2) concentrated HNO_3 at 115 °C for 10 min;
(3) HCl:H_2O_2:H_2O=1:1:5 at 80 °C for 10 min.
Hereafter, the oxide layers formed in solutions (1), (2), and (3) are referred to as H_2SO_4 oxide, HNO_3 oxide, and HCl oxide, respectively. After achieving ohmic contact at the rear silicon surface with In-Ga alloy, a ~ 3 nm-thick Pt layer was deposited on the oxide surface.

XPS spectra were measured using a VG SCIENTIFIC ESCALAB 220i-XL spectrometer with a monochromatized Al $K\alpha$ radiation source. For XPS measurements under bias, the front Pt layer was grounded and a bias voltage was applied to the rear silicon surface. X-ray was irradiated from the Pt-layer side at the incident angle of 45°, and photoelectrons were collected in the surface-normal direction.

FT-IR-ATR spectra were recorded in a dry nitrogen atmosphere using a BIORAD FTS-7 spectrometer. In the measurements, the Si wafers were attached to both sides of a Ge crystal with edges cut at 60°. The energy resolution was set at 4 cm^{-1}, and both *p*- and *s*-polarized incident light beams were employed.

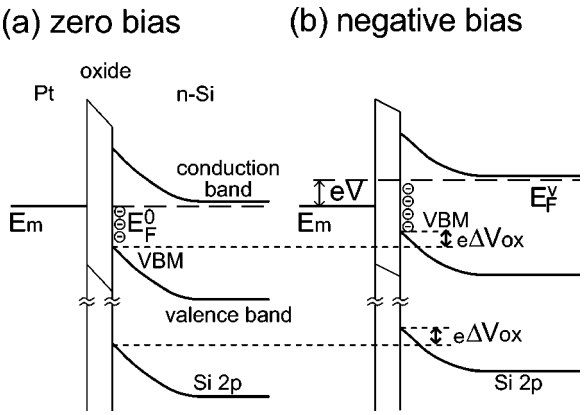

FIG. 1. Band diagrams for the *n*-Si-based MOS structure: (a) at zero bias; (b) under a negative bias applied to the Si with respect to the metal.

AFM measurements were performed with a Digital Instruments III A microscope, using a tapping mode in order to avoid surface damages. The scan area was $0.4\times 0.4\ \mu$m^2. The surfaces before and after oxidation as well as the Si surfaces after the etch of the oxide layer away with a 0.5% HF solution were investigated.

Synchrotron radiation UPS measurements were performed using a BL-3B beam line of Photon Factory at High-Energy Accelerator Research Organization. The incident photon energy was set at 170 or 130 eV, and photoelectron energies were analyzed using a double-path cylindrical mirror analyzer.

III. THEORETICAL PRINCIPLE

Figure 1 shows the band diagram of *n*-type Si-based MOS structure. The work function of Si is assumed to be higher than that of metal, inducing upward band bending in the Si due to positive charges of ionized donors. At zero bias, the Si Fermi level E_F^0, coincides with the metal Fermi level E_m [Fig. 1(a)]. In this case, interface states present below the Fermi level are occupied by electrons while those above the Fermi level are empty. By the application of a negative (or positive) bias V to the Si with respect to the metal layer, the Si Fermi level E_F^V is shifted upward (or downward) from the metal Fermi level E_m. Consequently, the interface states present between E_F^V and E_F^0 are newly occupied (or unoccupied) by electrons. This charge accumulated in the interface states $\Delta Q_{\rm it}$ induces a change in the potential drop across the oxide layer with the magnitude given by

$$\Delta V_{\rm ox}=\Delta Q_{\rm it}/C_{\rm ox}=\int_{E_F^0}^{E_F^V} D_{\rm it}(E)dx/C_{\rm ox}, \qquad (1)$$

where $C_{\rm ox}$ is the capacitance of the oxide layer, $D_{\rm it}$ is the density of the interface states as a function of energy E in the Si band gap, and the Si valence-band maximum is referred to as the energy standard. Since the energy difference between the oxide band and the Si $2p$ level at the interface is constant, the Si $2p$ level is shifted by the same magnitude as

ΔV_{ox}. This shift in the Si $2p$ level caused by the charge accumulated in the interface states by the bias is measurable by means of XPS.

Since the depletion layer width is much longer (e.g., ~ 1 μm for the Si with the donor density of $5\times10^{14}\,\mathrm{cm}^{-3}$ used in the present study) than the mean-free path of photoelectrons, the band in the region from which the photoelectron signal is observed can be considered to be flat. Therefore, the observed energy shift of the Si $2p$ peak is identical to the change in the potential drop across the oxide layer ΔV_{ox}.

On the other hand, the Fermi level under bias E_F^V is given by

$$E_F^V = E_F^0 - eV + e\Delta V_{ox}. \tag{2}$$

By use of Eqs. (1) and (2), D_{it} can be obtained as a function of E from measurements of the bias-induced energy shift of the Si $2p$ level ΔV_{ox} as a function of the bias voltage V. In the present study, C_{ox} and E_F^0 are determined from the electrical measurements.

IV. RESULTS

Figure 2 shows the AFM micrographs of atomically rough [Figs. 2(a)–2(c)] and smooth [Figs. 2(d)–2(f)] Si(111) surfaces, measured before and after oxidation with a concentrated HNO_3 solution, as an example. For an atomically rough surface, steps were not seen. When an atomically smooth Si(111) surface was produced, on the other hand, steps were clearly observed. The step height was 0.31 nm, which corresponded to Si double layers. The observation of the steps after the formation of the oxide layer [Fig. 2(e)] and after the etch of the oxide layer away [Fig. 2(f)] showed layer-by-layer oxidation using the chemical solution. Similar steps were also observed after oxidation with $HCl+H_2O_2$ and $H_2SO_4+H_2O_2$ and after the etch of these oxide layers away.

The root-mean square (Rms) roughness values for all the oxide layers are summarized in Table I. The Rms value of the atomically rough and smooth Si(111) surfaces before oxidation were 0.190 and 0.092 nm, respectively. After oxidation of the atomically rough surface, the Rms value remained nearly unchanged (i.e., 0.194 nm for HCl oxide, 0.190 nm for HNO_3 oxide, and 0.193 nm for H_2SO_4 oxide). The Rms values measured after the etch of the oxide layers away, on the other hand, strongly depended on the oxide types (i.e., 0.152 nm for HCl oxide, 0.195 nm for HNO_3 oxide, and 0.180 nm for H_2SO_4 oxide). These results indicate that the oxide/Si interface became smoother and rougher by the oxidation with $HCl+H_2O_2$ and HNO_3, respectively.

For the atomically smooth surface, the Rms roughness value was slightly increased after oxidation (i.e., 0.096 nm for HCl oxide, 0.122 nm for HNO_3 oxide, and 0.126 nm for H_2SO_4 oxide). After the etch of the oxide layers away, the Rms value was slightly decreased for HCl oxide (0.094 nm), while it was slightly increased for HNO_3 oxide (0.160 nm) and H_2SO_4 oxide (0.139 nm). These changes in the Rms value for the atomically smooth surface were similar to those for the atomically rough surface, also showing that the interface became smoother by oxidation with $HCl+H_2O_2$, while it became rougher by oxidation with HNO_3 and $H_2SO_4+H_2O_2$.

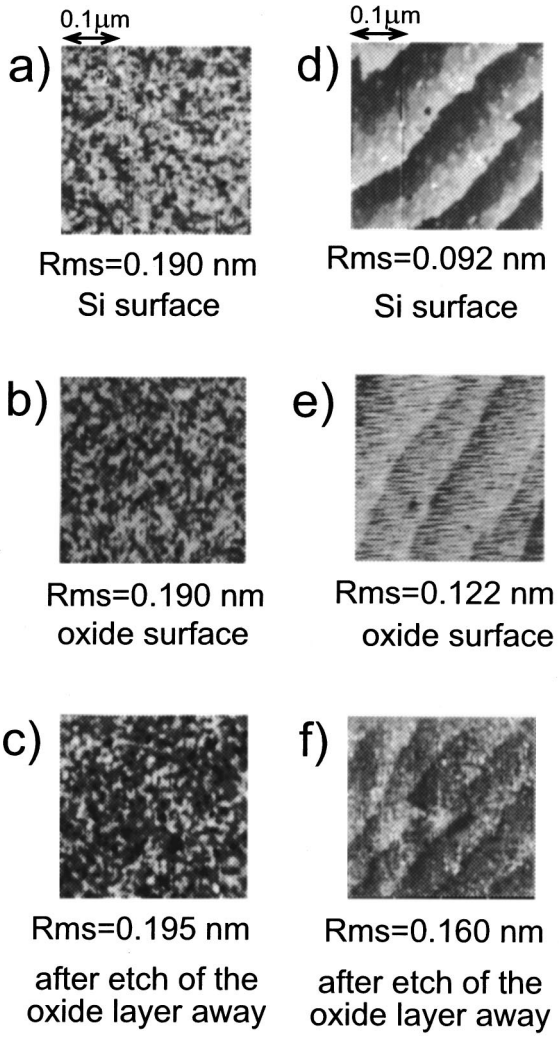

FIG. 2. AFM images ($0.4\times0.4\,\mu\mathrm{m}^2$) for the following Si(111) surfaces: (a) atomically rough surface before oxidation; (b) atomically rough surface after oxidation with the HNO_3 solution; (c) atomically rough surface after the etch of the oxide layer away; (d) atomically smooth surface before oxidation; (e) atomically smooth surface after oxidation with the HNO_3 solution; (f) atomically smooth surface after the etch of the oxide layer away.

Figure 3 shows the XPS spectra in the Si $2p$ region for the ⟨Pt/ultrathin oxide/Si(111)⟩ MOS structure. The doublet peaks were due to the Si $2p_{3/2}$ and $2p_{1/2}$ levels of the substrate and the broad peak was due to the oxide layer. From the ratio in the area intensity of the oxide peak to that of the substrate peaks, the thickness of the oxide layer was estimated to be 2.2 nm. In the estimation, 2.7 and 3.5 nm were used as the mean-free paths of photoelectrons in the Si substrate and the oxide layer, respectively.[19]

By the application of a positive bias voltage to the Si with respect to the Pt overlayer, the Si $2p$ peaks of the substrate were shifted toward the higher binding energy [Fig. 3(b)]. By the application of a negative bias voltage to the Si, on the other hand, the Si $2p$ peaks were shifted toward the lower binding energy [Fig. 3(c)]. These bias-induced shifts were completely reversible, that is to say, by the removal of the bias voltage, the shift always diminished. Therefore, the

TABLE I. The rms values (nm) measured after oxidation and the etch of the oxide layer away: (a) for the atomically rough Si(111); (b) for the atomically smooth Si(111). The rms values of the atomically rough and smooth Si(111) surfaces before oxidation were 0.190 and 0.092 nm, respectively.

(a) atomically rough Si	HCl oxide	HNO_3 oxide	H_2SO_4 oxide
After oxidation	0.194	0.190	0.193
After the etch of the oxide layer away	0.152	0.195	0.180

(b) atomically smooth Si	HCl oxide	HNO_3 oxide	H_2SO_4 oxide
After oxidation	0.096	0.122	0.126
After the etch of the oxide layer away	0.094	0.160	0.139

shifts were not due to chemical shifts but were caused by charges accumulated in the interface states by the bias.

Figure 4 shows the plots of the energy shift of the substrate Si $2p$ peak as a function of the bias voltage. For all the specimens investigated, the direction of the energy shifts was the same. However, the features of the plots depended on the oxide formation method. From the slope of the plots, the interface state density can be calculated using Eqs. (1) and (2). It should be noted that there were several bias regions where the shift completely stopped. These regions correspond to the energy regimes with no interface states.

Figure 5 shows the energy distribution of interface states for the MOS devices fabricated using the rough Si(111) surfaces, obtained from the analysis of Fig. 4. All the observed interface state spectra had peaked structure (not *U*-shaped energy distribution), indicating that they were due to defects

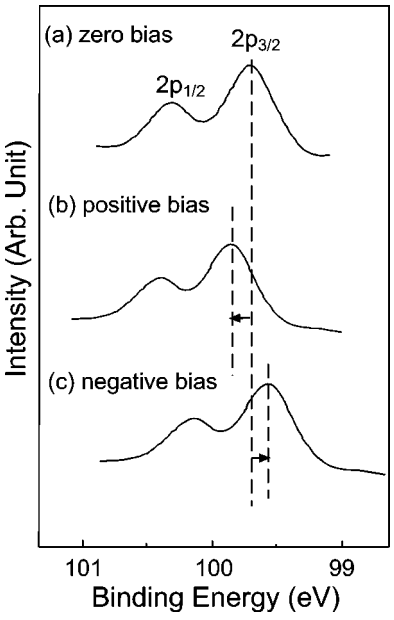

FIG. 3. XPS spectra in the Si $2p$ region for the atomically rough Si(111)-based MOS structure with an ultrathin chemical oxide layer formed in the HNO_3 solution: (a) at zero bias; (b) at 0.46 V applied to the Si with respect to the Pt; (c) at -0.43 V.

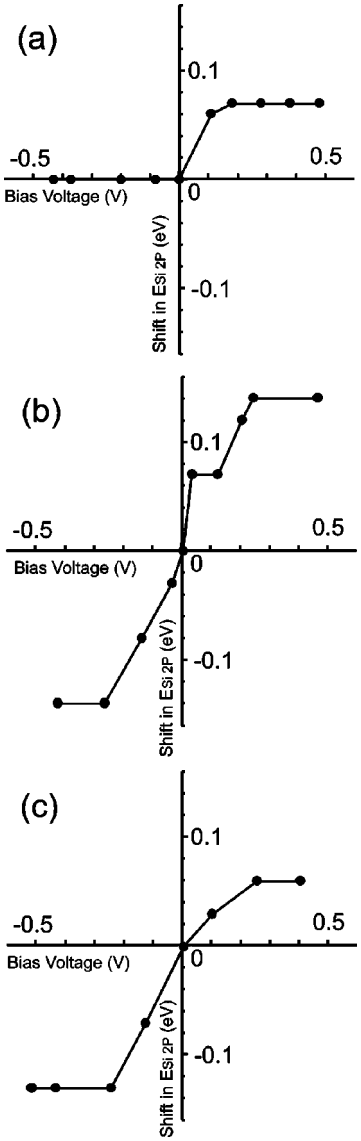

FIG. 4. Plots of the energy shifts of the substrate Si $2p$ peak for the atomically rough Si(111)-based MOS structure with an ultrathin chemical oxide layer formed in the following solutions vs the bias voltage: (a) $HCl+H_2O_2$; (b) HNO_3; (c) $H_2SO_4+H_2O_2$.

such as silicon dangling bonds. Calculations recently performed by us using a density-functional theory method have shown that an isolated silicon dangling bond has an energy level near the midgap, while a silicon dangling bond interacting weakly with a Si or oxygen atom having lone-pair electrons (or an unpaired electron) in the oxide layer possesses an energy level above (or below) the midgap.[20] Therefore, the interface state peak observed near the midgap for the HCl oxide layer [Fig. 5(a)] is attributable to isolated Si dangling bonds. The interface state peaks above and below the midgap for the HNO_3 oxide layer [Fig. 5(b)] are attributable to Si dangling bonds interacting weakly with a Si or oxygen atom in the oxide layer. The broad interface state peak for the H_2SO_4 oxide layer [Fig. 5(c)] is attributed to these three kinds of interface states overlapping with one another.

Figure 6 shows the energy distribution of interface states for the MOS devices produced from the atomically smooth Si(111) surfaces. The interface state density for the atomi-

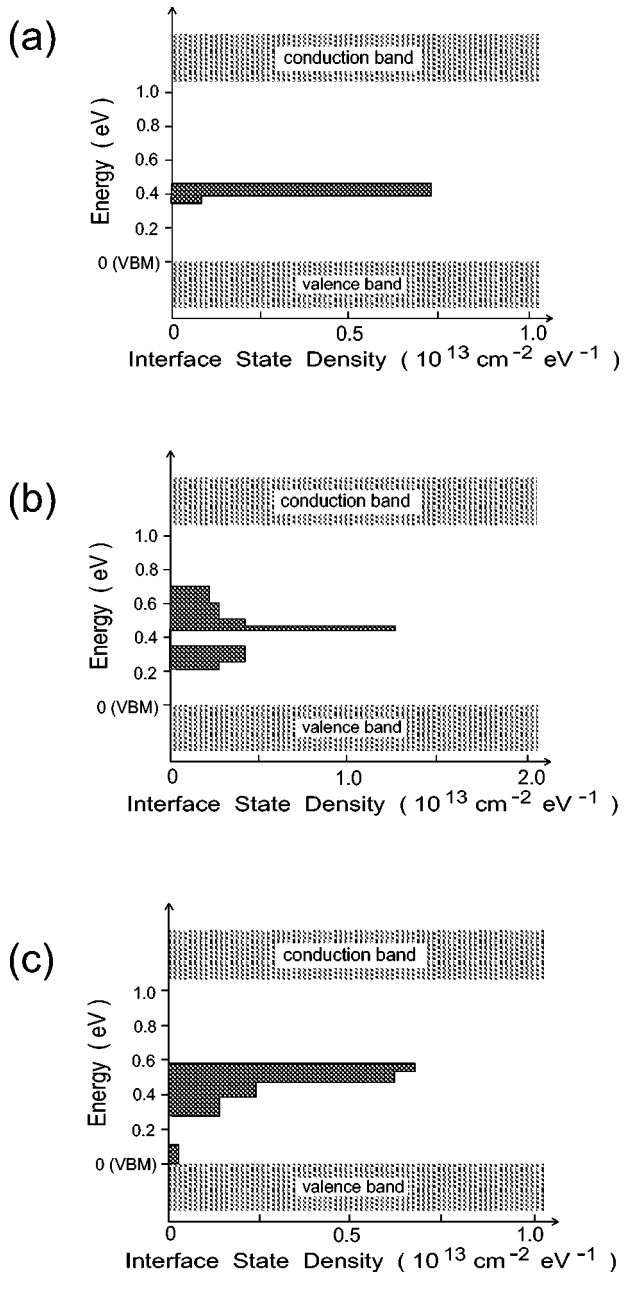

FIG. 5. Energy distribution of interface states for the atomically rough Si(111)-based MOS devices with an ultrathin chemical oxide layer formed in the following solutions: (a) $HCl+H_2O_2$; (b) HNO_3; (c) $H_2SO_4+H_2O_2$.

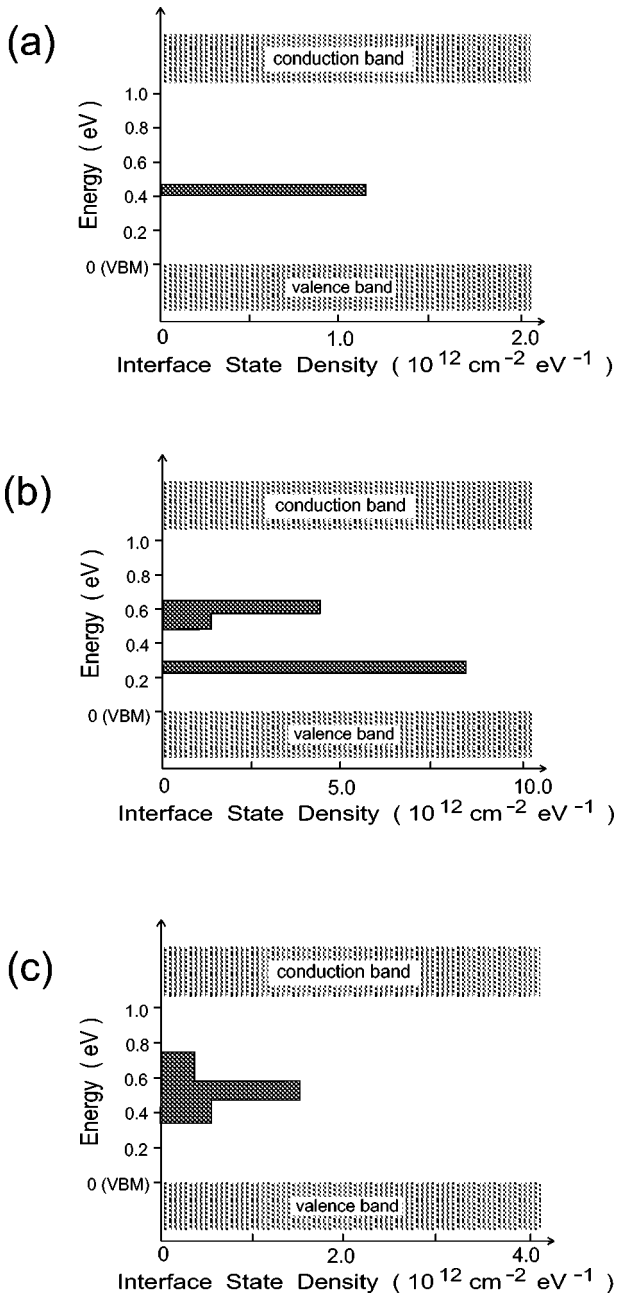

FIG. 6. Energy distribution of interface states for the atomically smooth Si(111)-based MOS devices with an ultrathin chemical oxide layer formed in the following solutions: (a) $HCl+H_2O_2$; (b) HNO_3; (c) $H_2SO_4+H_2O_2$.

cally smooth interfaces was much lower than that for the rough interfaces. On the other hand, the energy distribution of the interface states for both interfaces was almost the same, and strongly depended on the kinds of the oxidizing solutions.

The total interface state densities for all the oxide layers investigated are summarized in Table II. The interface state density for the atomically smooth interface was always lower than that for the atomically rough interface. (In particular, the interface state density for HCl oxide was decreased to ~1/8 by the formation of the atomically smooth interface.) When the initial surface roughness before oxidation was the same, the interface state density for the HCl oxide layer was the lowest, while that for the HNO_3 oxide layer was the highest. It should be noted that the interface state density obtained from XPS measurements under bias is one or two orders of magnitude higher than that examined using electrical technique probably because all interface states having various time constants are detected.

TABLE II. Total interface states densities, N_{rough} and N_{smooth}, for atomically rough and smooth Si/oxide interfaces, respectively.

	HCl oxide	HNO_3 oxide	H_2SO_4 oxide
$N_{rough}(\times 10^{12}\,cm^{-2})$	0.48	1.8	1.3
$N_{smooth}(\times 10^{12}\,cm^{-2})$	0.06	0.75	0.27

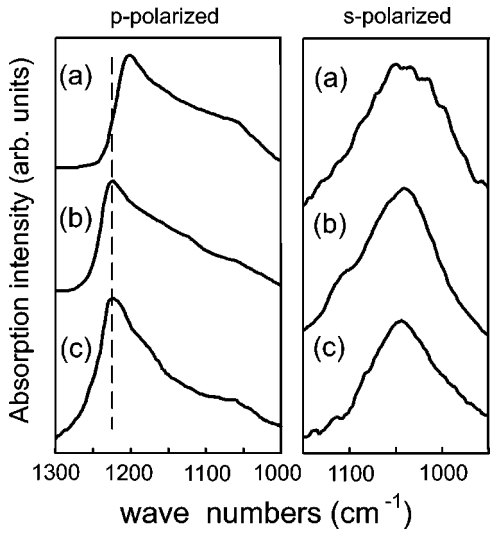

FIG. 7. FT-IR-ATR spectra for the ultrathin chemical oxide layers formed in the following solutions on the Si(111) substrate: (a) $HCl+H_2O_2$; (b) HNO_3; (c) $H_2SO_4+H_2O_2$.

Figure 7 shows the FT-IR-ATR spectra for the chemical oxide layers formed on the Si(111) substrate. The vibrational energy of the longitudinal optical (LO) mode depended on the oxide types (1197 cm^{-1} for HCl oxide, and 1226 cm^{-1} for HNO_3 and H_2SO_4 oxides), while that of the transverse optical (TO) mode nominally depended on it (i.e., 1050 cm^{-1} for all the oxide layers).

Figure 8 shows the synchrotron radiation UPS spectra in the Si $2p$ region for the HCl oxide layer formed on the atomically rough Si(111) surface, measured at 170 [spectrum (a)] and 130 eV [spectrum (b)] photon energies. In the curve resolution method, the background was removed using a following method. The background curves were obtained by measurements of the UPS spectra using 10 eV lower energy photons. Then, the background was subtracted from the corresponding Si $2p$ spectra. The background intensity due to the inelastic scattering of the Si $2p$ photoelectrons was estimated by use of the Shirley method, i.e., the method in which the loss intensity at binding energy E was assumed to be proportional to the integral of the Si $2p$ photoelectron intensity in the energy region lower than E. After the subtraction of the background, peaks due to the Si $2p_{1/2}$ components were mathematically removed, considering that the Si $2p_{1/2}$ levels had intensities a half the corresponding Si $2p_{3/2}$ levels and the energy difference between both levels was 0.61 eV, and thus only the Si $2p_{3/2}$ components were indicated in Fig. 5 for simplicity. In the figure, Si^0 and Si^{4+} denote the Si substrate and SiO_2, respectively, and Si^{1+}, Si^{2+}, and Si^{3+} denote Si atoms bound to one, two, and three oxygen atoms, respectively. The energies and the widths of the suboxide Si $2p$ peaks did not depend on the oxide formation methods and the incident photon energies, indicating that the curve resolution method was unique. It is seen from Fig. 8 that the Si $2p$ peaks due to the suboxide species were present with considerably high intensities.

The deconvolution of the UPS spectra also shows that the oxide layers contained considerable amounts of Si-H species whose Si $2p$ peak was present at ~0.4 eV with respect to the substrate Si $2p$ peak.[21,22]

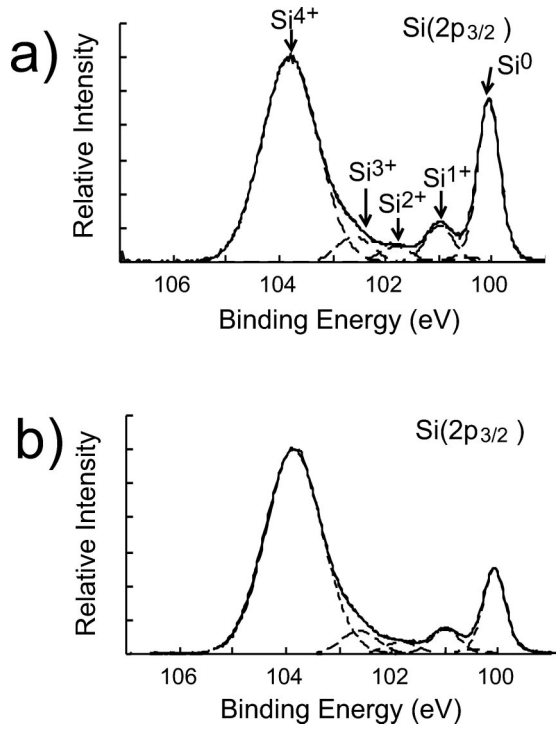

FIG. 8. Synchrotron radiation UPS spectra in the Si $2p$ region for the ultrathin chemical oxide layer formed by the immersion of the atomically rough Si(111) in $HCl+H_2O_2$. Spectra (a) and (b) were measured at the photon energy of 170 and 130 eV, respectively.

Table III shows the ratio in the intensity of the suboxide Si $2p$ peak to that of the Si^{4+} peak. Since Si^{4+} is the main component of the oxide layer and it is present almost uniformly in the oxide layer, the ratio gives the information where the suboxide species is mainly present. Although the relative intensities of the suboxide peaks changed by ±15% from sample to sample, those of the Si^{1+} and Si^{2+} peaks measured at 170 eV incident photon energy were always higher than those measured at 130 eV. Since the mean-free path of photoelectrons excited by 170 eV photons (~0.4 nm) is longer than that excited by 130 eV photons (~0.3 nm),[23] this result shows that the concentrations of the Si^{1+} and Si^{2+} species were high near the oxide/Si interface. On the other hand, the relative intensity of the Si^{3+} peak observed at 170 eV was not always higher than that observed at 130 eV, showing that the concentration of the Si^{3+} species was not high at the interface.

It is seen from Table III that the oxide layers contained a considerable amount of the Si-H species. The intensity of the Si-H peak increased by use of 170 eV energy photons only for the HNO_3 oxide layer. For the HCl oxide layer, on the other hand, the intensity of the Si-H peak was almost unchanged using 170 eV energy photons, or even decreased for the H_2SO_4 oxide layer. These results show that the concentration of the Si-H species at the interface was high only for the HNO_3 oxide layer.

Table IV compares the intensities of the Si^{2+} and Si^{1+} peaks normalized by that of the substrate peak for the smooth interfaces with those for the rough interfaces, measured at the 170 eV photon energy. The relative intensity of the Si^{2+} peak was always decreased by the formation of the

TABLE III. Ratios in the intensity of the Si $2p$ peak of the suboxide and Si-H species to that of the Si^{4+} species.

	HCl oxide		HNO_3 oxide		H_2SO_4 oxide	
	130 eV	170 eV	130 eV	170 eV	130 eV	170 eV
Si^{1+}	0.068	0.119	0.015	0.019	0.026	0.051
Si^{2+}	0.26	0.046	0.014	0.017	0.018	0.026
Si^{3+}	0.078	0.103	0.036	0.030	0.045	0.064
Si-H	0.005	0.006	0.005	0.008	0.006	0.005

smooth interface, while that of the Si^{1+} peak was not always decreased. Comparison of Table IV with Table II shows that the total interface state density has a good relation with the amount of the Si^{2+} species, but not with that of the Si^{1+} species.

Photon energy-dependent measurements of the UPS spectra show that the Si^{3+} species does not have a high concentration near the interface but has a rather uniform concentration in the oxide layer. Therefore, the relative intensity of the Si^{3+} peak with respect to the substrate peak has no physical meaning and thus it is not included in Table IV.

V. DISCUSSION

A. Interface state density and the interfacial roughness

The Rms roughness values observed after the etch of the oxide layer away differ only slightly from that before oxidation. This result indicates that the roughness at the oxide/Si interface is strongly dependent of the initial surface roughness. The interface state density for the MOS devices fabricated from the atomically smooth Si surface is always lower than that produced from the rough Si surface (cf. Table II). Therefore, it can be concluded that the interface state density greatly depends on the interfacial roughness.

Among the oxide layers formed from the atomically rough Si surface, the HCl oxide layer has the lowest Rms roughness value (0.152 nm) after the etch of the oxide layer away and it also has the lowest interface state density, N_{it} ($4.8\times10^{11}\,cm^{-2}$), while the HNO_3 oxide layer has the highest Rms value (0.195 nm) and the highest interface state density ($1.8\times10^{12}\,cm^{-2}$).

$$\mathrm{Rms}(HNO_3\ \mathrm{oxide})>\mathrm{Rms}(H_2SO_4\ \mathrm{oxide})>\mathrm{Rms}(\mathrm{HCI\ oxide}), \tag{3}$$

$$N_{it}(HNO_3\ \mathrm{oxide})>N_{it}(H_2SO_4\ \mathrm{oxide})>N_{it}(\mathrm{HCl\ oxide}). \tag{4}$$

The oxide layers formed from the atomically smooth Si surface also have the same orders in Rms and N_{it}. These results also strongly indicate a strong relation between the interface state density and the interfacial roughness.

B. Amount of the Si^{2+} species and the interface state density

The photon energy-dependent measurements of the UPS spectra show that the amounts of the Si^{2+} and Si^{1+} species are high near the interface while the Si^{3+} species is present more uniformly in the silicon oxide layer. It is found that the interface state density strongly correlates with the amount of the Si^{2+} species as explained below, while there is no relation between the amounts of the Si^{1+} and Si^{3+} species and the interface state density.

The amount of the Si^{2+} species is always decreased to a small extent by the formation of the atomically flat interfaces, as is evident from Table IV. The small decrease is likely to result from a vast reduction in the amount of Si^{2+} in the interfacial region with its amount in the oxide bulk nearly unchanged. Since the interface state density for the atomically smooth interfaces is always lower than that for the rough interfaces, it can be concluded that there is correlation between the interface state density and the amount of the Si^{2+} species at the interface.

For both atomically smooth and rough interfaces, the amount of the Si^{2+} species c_{Si2+} is in the following order (cf. Table IV);

$$c_{Si2+}(HNO_3\ \mathrm{oxide})>c_{Si2+}(H_2SO_4\ \mathrm{oxide})>c_{Si2+}(\mathrm{HCl\ oxide}). \tag{5}$$

For both interfaces, the interface state density N_{it} has the same order as shown in Eq. (4). These results also show the good correlation between the amount of the Si^{2+} species and the interface state density.

It is very likely that the Si^{2+} species present at the rough interfaces is mainly due to step edges [cf., Fig. 9(a)]. Therefore, the decrease in the amount of Si^{2+} by the formation of the atomically smooth interfaces is attributable to a reduction in the density of the bilayer steps. We think that the bilayer

TABLE IV. Ratios in the area intensity of the Si $2p$ peak of the Si^{2+} and Si^{2+} species to that of the Si substrate.

	HCl oxide		HNO_3 oxide		H_2SO_4 oxide	
	Rough	Smooth	Rough	Smooth	Rough	Smooth
Si^{2+}	0.12	0.10	0.22	0.20	0.17	0.11
Si^{1+}	0.25	0.26	0.27	0.23	0.15	0.22

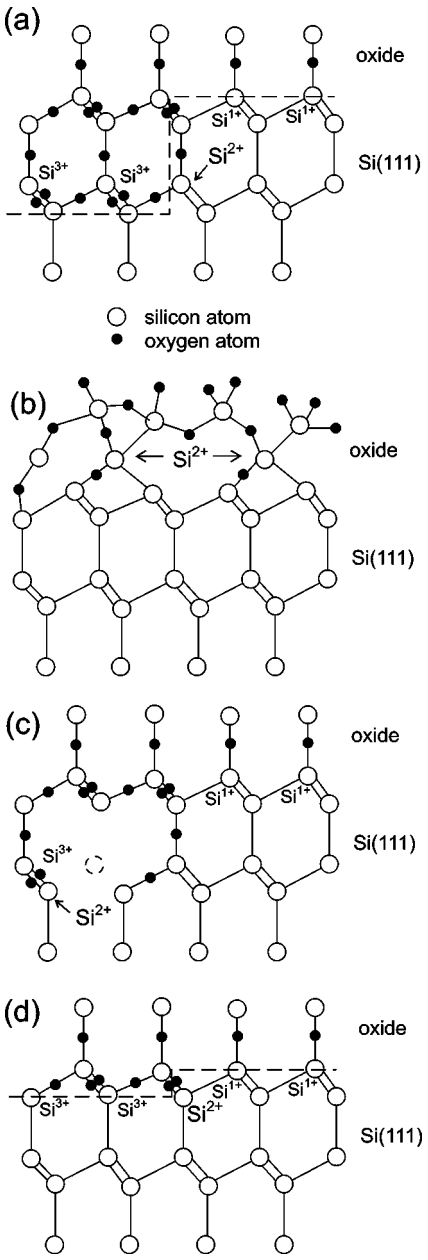

FIG. 9. Possible structural imperfections which include Si^{2+} species, at oxide/Si(111) interfaces: (a) bilayer steps; (b) stacking faultlike defects; (c) vacancylike defects; (d) monolayer steplike defects. Si^{+}, Si^{2+}, and Si^{3+} denote Si atoms bound to one, two, and three oxygen atoms, respectively.

steps hinder the formation of complete SiO_2 networks, and consequently the Si dangling bond interface states are generated near the steps.

For the atomically smooth Si(111) surface, the bilayer steps were observed before and after oxidation, and after the etch of the oxide layer away, irrespective of the oxide types. Considering that the terrace width is ~ 0.1 μm, the density of the step atoms is estimated to be $5.2\times10^{12}\,\mathrm{cm}^{-2}$ (6.7×10^{-3} monolayer). Since these steps arise from a misorientation of the surface from the (111) orientation, the step density does not depend on the oxide types. Therefore, the difference in the Rms value among the oxide layers with the smooth interface is not attributable to the bilayer steps.

It is observed that among the oxide layers with the smooth interfaces, the amount of the Si^{2+} species increases with the Rms roughness value. This variation in the amount of Si^{2+} is not attributable to the bilayer steps, as explained above. There are several possibilities for the origin of Si^{2+} at the interface: (i) stacking faultlike defects [Fig. 9(b)], (ii) vacancylike defects [Fig. 9(c)], and (iii) monolayer steplike structure of the oxide/Si interface [Fig. 9(d)] resulting from nonuniform oxidation. These defects cause the microroughness (thus well explaining the good relation between the amount of the Si^{2+} species and the Rms roughness value), and prevent the formation of complete SiO_2 networks, resulting in the Si dangling bond interface states.

C. Energy of the interface states and atomic density of the oxide layers

The energy distribution of the interface states strongly depends on the oxide type (i.e., one sharp peak for the HCl oxide layer, two sharp peaks for the HNO_3 oxide layer, and one broad peak for the H_2SO_4 oxide layer), but not on the interfacial roughness. We conclude that the variation in the energy distribution of the interface states results from the difference in the properties of the chemical oxide layers, (especially the atomic density) as explained below.

The vibrational energy of LO phonons depends on the oxide type while that of TO phonons does not depend on it (Fig. 7). The relation in the angular frequency between LO (ω_{LO}) and TO (ω_{TO}) phonons of the asymmetric Si-O stretching vibration is expressed as[24,25]

$$\omega_{\mathrm{LO}}^2-\omega_{\mathrm{TO}}^2=2\gamma/m, \tag{6}$$

where m is the mass of an oxygen atom, and γ is an electric term given by

$$\gamma=Z^2\rho/[\varepsilon\varepsilon_0(2m+M)], \tag{7}$$

where ε and ε_0 are the relative dielectric constant of the oxide layer and the permittivity of vacuum, respectively, M is the mass of a Si atom, Z is a dynamical charge for the Si-O vibration, and ρ is the atomic density of the oxide layer.

The relation between ε and ρ is given by

$$\varepsilon=1+C_1\rho, \tag{8}$$

where C_1 is a constant. Using Eqs. (7) and (8), Eq. (6) reduces to

$$\omega_{\mathrm{LO}}^2-\omega_{\mathrm{TO}}^2=\frac{2Z^2}{m(2m+M)}\cdot\frac{\rho}{\varepsilon_0(1+C_1\rho)}=\frac{C_2\rho}{1+C_1\rho}, \tag{9}$$

showing that $\omega_{\mathrm{LO}}^2-\omega_{\mathrm{TO}}^2$ monotonically increases with the oxide atomic density ρ. From the values of thick thermal oxide layers, i.e., 3.9 as ε, $2.28\times10^{22}\,\mathrm{cm}^3$ as ρ, 1255 and 1070 cm^{-1} as the wave numbers of LO and TO phonons, respectively,[26] C_1 and C_2 are estimated to be $1.3\times10^{-22}\,\mathrm{cm}^3$ and $7.4\times10^{-17}\,\mathrm{cm}^2$, respectively. ω_{LO} for the HCl oxide layer (1197 cm^{-1}) is lower than that for the HNO_3 and H_2SO_4 oxide layers (1226 cm^{-1}), while ω_{TO} is identical to one another. Using these values in Eq. (9), the atomic densities of the HCl, H_2SO_4, and HNO_3 oxide layers are estimated to be 2.01×10^{22}, 2.21×10^{22}, and $2.21\times10^{22}\,\mathrm{cm}^{-3}$, respectively (i.e., the atomic density of the

HNO_3 and H_2SO_4 oxide layers is ~1.1 times that of the HCl oxide layer). Sugita, Watanabe, and Awaji[27] also observed that the vibrational energy of LO phonons increased with the oxide density, while that of TO phonons depends nominally on it. They also concluded from the FT-IR as well as x-ray reflectometry results that the density of the HCl oxide layer was lower than those of the HNO_3 and H_2SO_4 oxide layers.

It is likely that the different atomic density of the oxide layer results in the variation in the distance between a Si dangling bond and the interacting atom in the oxide layer. When the oxide layer has a low atomic density (e.g., HCl oxide), a Si dangling bond has a large space (i.e., long distance between the Si dangling bond and the atom in the oxide layer), resulting in an isolated silicon dangling bond state. Consequently, the interface state peak appears near the midgap [Fig. 5(a)]. For a high-atomic density oxide layer (e.g., HNO_3 oxide), on the other hand, a Si or oxygen atom in the oxide layer is present near the Si dangling bond and interacts weakly. Due to the weak interaction, the energy level of the Si dangling bond shifts upward or downward depending on whether the interacting atom has lone-pair electrons or an unpaired electron [Fig. 5(b)].

Although the atomic density obtained from the FT-IR measurements is the same for the HNO_3 and H_2SO_4 oxide layers, the energy distribution of the interface states is different from each other [Figs. 5(b) and 5(c)]. This difference in the interface states is attributable to the variation in the amount of the Si-H species, as explained below. The photon energy-dependent UPS measurements show that the amount of the Si-H species at the interface is high only for the HNO_3 oxide layer (Table III). It is very likely that the Si dangling bonds at the interface for the HNO_3 oxide layer are terminated by hydrogen atoms. Since an isolated Si dangling bond possesses a large space, the Si-H bond is more easily formed from it than from the dangling bond interacting weakly with an atom in the oxide layer, and consequently the interface states near the midgap is removed, resulting in the two-peaked structure of the interface state spectrum.

The above conclusion that the energy distribution of interface states strongly depends on the atomic density of the silicon oxide layer is supported by the interface state spectra for thermal and native oxide layers previously observed by us.[6,10] For the native oxide layer, which is likely to have a low-atomic density, an interface state peak due to isolated Si dangling bond states is observed near the midgap. For the thermal oxide layer formed at 450 °C, the interface state peak near the midgap is considerably broaden due to the weak interaction between the Si dangling bond and the atom in the oxide, showing that the low-temperature thermal oxide layer has a higher atomic density than the native oxide layer. When the formation temperature of the thermal oxide layer is increased to 650 °C, two interface state peaks (one above and the other below the midgap) due to Si dangling bonds weakly interacting with a Si or oxygen atom in the oxide layer are present because of a further increase in the atomic density of the oxide layer.

VI. CONCLUSION

From the analysis of the interface state spectra for the ultrathin oxide/Si interfaces determined from XPS measurements under bias, together with the FT-IR-ATR, AFM, and synchrotron UPS results, we have concluded that the density of the interface states present at the silicon oxide/Si interface depends on the interfacial roughness, while the energy distribution on the atomic density of the oxide layer:

(1) The interface state density for the atomically smooth interface is in much lower than that for the rough interface.

(2) The interface becomes smoother than the initial Si (111) surface after oxidation with the $HCl+H_2O_2$ solution, while it is made rougher by oxidation with the $H_2SO_4+H_2O_2$ or HNO_3 solution. Consequently, the HCl oxide layer has a lower interface state density than the H_2SO_4 and HNO_3 oxide layers.

(3) There is a strong relation between the amount of the Si^{2+} species in the interfacial region and the interface state density. The Si^{2+} species is present in structural imperfect regions such as step edges, and thus the relation is considered to show that the interface states are formed near the structural imperfect places.

(4) From the energy difference between LO and TO phonons of the Si-O vibration, the atomic density of the HNO_3 oxide and H_2SO_4 oxide layers is estimated to be ~1.1 times that of the HCl oxide layer.

(5) In cases where the oxide layer has a low-atomic density (e.g., HCl oxide), an interface state peak due to isolated Si dangling bonds appears near the midgap. For the high-density oxide layers (e.g., HNO_3 oxide layer), on the other hand, interface state peaks are present above and below the midgap because of the weak interaction between a Si dangling bond and a Si or oxygen atom in the oxide layer.

ACKNOWLEDGMENT

A part of this work was supported by ASET, NEDO.

[1] E. H. Nicollian and J. R. Brews, *MOS (Metal Oxide Semiconductor) Physics and Technology* (Wiley, New York, 1982).

[2] C. N. Berglund, IEEE Trans. Electron Devices **ED-13**, 701 (1996).

[3] L. M. Terman, Solid-State Electron. **5**, 285 (1962).

[4] E. H. Nicollian and A. Goetzberger, Bell Syst. Tech. J. **46**, 1055 (1967).

[5] H. S. Haddara and M. El-Sayed, Solid-State Electron. **31**, 1289 (1988).

[6] H. Kobayashi, Y. Yamashita, T. Mori, Y. Nakato, K. H. Park, and Y. Nishioka, Surf. Sci. **326**, 124 (1995).

[7] H. Kobayashi, T. Mori, K. Namba, and Y. Nakato, Solid State Commun. **92**, 249 (1994).

[8] H. Kobayashi, K. Namba, T. Mori, and Y. Nakato, Phys. Rev. B **52**, 5781 (1995).

[9] Y. Yamashita, K. Namba, Y. Nakato, Y. Nishioka, and H. Kobayashi, J. Appl. Phys. **79**, 7051 (1996).

[10] H. Kobayashi, A. Asano, S. Asada, T. Kubota, Y. Yamashita, K. Yoneda, and Y. Todokoro, J. Appl. Phys. **83**, 2098 (1998).

[11] H. Kobayashi, K. Namba, Y. Yamashita, Y. Nakato, T. Komeda,

and Y. Nishioka, J. Appl. Phys. **80**, 1578 (1996).
[12] N. M. Johnson, D. K. Biegelsen, M. D. Moyer, S. T. Chang, E. H. Poindexter, and P. J. Caplan, Appl. Phys. Lett. **43**, 563 (1983).
[13] E. H. Poindexter, G. J. Gerardi, M.-E. Rueckel, P. J. Caplan, N. M. Johnson, and D. K. Biegelsen, J. Appl. Phys. **56**, 2844 (1984).
[14] C. H. Bjorkman, T. Yasuda, C. E. Shearon, Jr., Y. Ma, G. Lucovsky, U. Emmerichs, C. Meyer, K. Leo, and H. Kurz, J. Vac. Sci. Technol. B **11**, 1521 (1993).
[15] T. Yasuda, Y. Ma, Y. L. Chen, G. Lucovsky, and D. Maher, J. Vac. Sci. Technol. A **11**, 945 (1993).
[16] T. Ohmi, M. Miyashita, M. Itano, T. Imaoka, and I. Kawanabe, IEEE Trans. Electron Devices **ED-39**, 537 (1992).
[17] P. O. Hahn and Henzler, J. Vac. Sci. Technol. A **2**, 574 (1984).
[18] G. S. Higashi, R. S. Becker, Y. J. Chabal, and A. J. Becker, Appl. Phys. Lett. **58**, 1656 (1991).
[19] M. Nishiyama, T. Mizokuro, K. Yoneda, and H. Kobayashi, Appl. Surf. Sci. **133**, 287 (1998).
[20] T. Kubota, A. Asano, Y. Nishioka, and H. Kobayashi (unpublished).
[21] C. U. S. Larsson, A. S. Flodström, R. Nyholm, L Incoccia, and F. Senf., J. Vac. Sci. Technol. A **5**, 3321 (1987).
[22] C. J. Karlsson, E. Landemark, L. S. O. Johansson, U. O. Karlsson, and R. I. G. Uhrberg, Phys. Rev. B **41**, 1521 (1990).
[23] F. J. Himpsel, F. R. McFeely, A. Taleb-Ibrahimi, J. A. Yarmoff, and G. Hollinger, Phys. Rev. B **38**, 6084 (1988).
[24] A. Lehmann, L. Schumann, and K. Hübner, Phys. Status Solidi B **117**, 689 (1983).
[25] R. A. B. Devine, Appl. Phys. Lett. **68**, 3108 (1996).
[26] Y. Sugita, S. Watanabe, N. Awaji, and S. Komiya, Appl. Surf. Sci. **100/101**, 268 (1996).
[27] Y. Sugita, S. Watanabe, and N. Awaji, Jpn. J. Appl. Phys., Part 1 **35**, 5437 (1996).